The effects of aspect ratio of inorganic fillers on the structure and property of composite ion-exchange membranes

Chalida Klaysom [a], Seung-Hyeon Moon [b], Bradley P. Ladewig [a,c], G.Q. Max Lu [a,*], Lianzhou Wang [a,*]

[a] ARC Centre of Excellence for Functional Nanomaterials, School of Chemical Engineering and Australian Institute of Bioengineering and Nanotechnology, The University of Queensland, Qld 4072, Australia
[b] Gwangju Institute of Science and Technology, School of Environmental Science and Engineering, Gwangju 500-712, Republic of Korea
[c] Monash University, Department of Chemical Engineering, Vic. 3800, Australia

ABSTRACT

A new type of nanocomposite ion-exchange membranes containing sulfonated polyethersulfone (sPES) polymer matrix and sulfonated surface-functionalized mesoporous silica (SS) inorganic fillers was prepared. Various characterizations revealed that the addition of inorganic fillers with different shapes had a significant influence on the membrane structure. The mesoporous inorganic fillers not only created extra pore and water channels, assisting the ionic migration and improving conductivity of the composites, but also provided additional fixed charge groups upon surface modification. This allows the Donnan exclusion to work effectively and thus improve the selectivity of membranes. It was proved that the incorporation of appropriate amount of SS additive could significantly improve the conductivity (up to 20 folds) and permselectivity (about 14%) of the sPES membranes. The performance of these newly developed membranes in desalination by electrodialysis was comparable with that of a commercial membrane (FKE).

© 2011 Elsevier Inc. All rights reserved.

1. Introduction

Recently, a number of polymer families have been widely developed to create desirable properties for use in ion-exchange membranes (IEMs) due to their versatile applications in research and industry including fuel cell, batteries, water purification, food and agricultural application, chemical industrial process, and desalination [1–12]. Among numerous polymers, polyether sulfone (PES) has been considered to be a good candidate because of its good chemical, thermal, and mechanical stabilities and ability for chemical modification on the aromatic rings of its polymer backbone.

In general, for electrodriving process, the IEMs are expected to possess excellent conductivity, high selectivity, and good chemical, thermal, and mechanical stabilities. To achieve the above mentioned properties, the PES requires a high level of chemical modification to introduce charged functional groups on the polymer backbone. Unfortunately, such a modification, normally via sulfonation reaction, results in a membrane that is mechanically weak and thus impractical for an application in electrodriving processes. Many strategies were applied in order to keep the sulfonated polyethersulfone (sPES) membranes highly conductive and selective, while retaining their mechanical stability. These included crosslinking of the sPES polymer chains, spacing the functional groups

on the polymer backbone with a hydrophobic unit, and introducing inorganic fillers [2]. Although the concept of composite has existed for some time, it has not been widely applied in membrane formation for the electrodriving membrane process such as electrodialysis (ED) desalination [13,14]. There were even rare studies investigating the influence of inorganic fillers on the structure and performance of composites. Thus, systematic investigation on the design and understanding of composite membranes suitable for a niche application is of high demand.

Material selection is one of the most important steps when developing a new membrane. Also, to systematically study the effects of the inorganic additives in the composites, a well-defined material with good potential for chemical modification is preferable. As they are easy to process and to reproduce with controlled size, shape, and surface functionalization, mesoporous silica nanoparticles are among the most versatile particles studied in the past decades. Recently, much research has focused on modifying mesoporous SiO_2 for a number of applications such as fuel cells [15]. More recent work focused on incorporating mesoporous $SO_3H–SiO_2$ (SS) into proton exchange membrane (PEM) fuel cells revealed that membrane performance has been significantly improved by incorporating these surface functionalized particles [16–19].

The main roles of the inorganic fillers in composite membranes are to retain water inside the membrane, to improve conductivity, and ion-exchange capacity (IEC), while maintaining good mechanical and thermal stability [2]. However, it is known that the inclusion

of inorganic fillers in polymer matrix would have a certain impact on the properties of the parent polymer. For instance, the fillers can alter the reology of the polymer matrix, thus leading to varied microstructures of the final products. Therefore, a number of important parameters such as surface functional groups, compositions and ratios of inorganic/organic components, and mixing procedure, etc., have to be carefully controlled. Among those parameters, the interfacial interaction between the components is considered to be critically important in determining the micro-structure and properties of the final products; equally important for the morphology/shape/size of the fillers, because it can change the interfacial interaction significantly [20]. Interestingly, the arrangement of the fillers in the matrix was also reported to have an important influence on the flux and selectivity in some membrane separation processes [21,22]. We were in interested in developing composite membranes using sulfonated PES (sPES) as the polymer matrix and mesoporous silica with different shapes and aspect ratios (length/diameter) as the inorganic fillers. In this work, the surface of inorganic fillers was modified with a sulfonate group in order to assist dispersion in the matrix polymer and also to provide additional charged functional groups to enhance the IEC, conductivity, and thus the selectivity of the membranes. The effects of aspect ratio of inorganic fillers on membrane structure, property, and performance, as an ion-selective membrane for desalination by ED, were investigated in detail. It was revealed that small amount of inorganic fillers with different aspect ratios could drastically change the physicochemical properties and electrotransport of ions of the composite membranes. The resultant composite membranes under optimized synthesis conditions offered comparable performance in desalination by electrodialysis with a commercial membrane (FKE).

2. Experimental

2.1. Preparation of the sulfonated mesoporous SiO$_2$

SO$_3$H-functionalized mesoporous SiO$_2$ was prepared by adapting the procedure described elsewhere [18,23]. Typically, the mixture of 300 cm^3 of DI water, 2.3 cm^3 of 2 mol dm^{-3} NaOH solution, 0.6 g of surfactant cetyltrimethylammonium bromide (CTAB, Aldrich), and 0.06 g of perfluorooctanoic acid (PFOA, Aldrich) was heated up to 60 °C or 80 °C under stirring. After a clear solution was obtained, 3.82 g of tetraethylorthosilicate (TEOS, Fluka) was added to the solution. After a defined reaction time between 5 and 60 s for the TEOS-containing mixture, an amount of mercaptopropyl trimethoxysilane (MPTMS, Sigma) equivalent 1:10 mol ratio MPTMS/TEOS was added and stirred for another 2 h. The synthesized powders were filtered and subsequently washed with DI water and ethanol. The template was removed by extraction in boiled acidified ethanol solution under reflux for 24 h. Then, 0.3 g of the as-synthesized powder was collected, dried, and re-dispersed in 10 cm^3 of H$_2$O$_2$ (30%, Ajax Finechem) at room temperature for 48 h. The suspended powders were centrifuged and added into 30 cm^3 of 1 mol dm^{-3} H$_2$SO$_4$ under stirring conditions for 2 h and then filtered and dried at room temperature. The ion-exchange capacity of the SO$_3$H-functionalized mesoporous SiO$_2$ was measured by back titration. The structure and morphology of the SO$_3$H–SiO$_2$ (SS) were studied by transmission electron microscopy (TEM, JEOL 1010) and X-ray diffraction (XRD, Rigaku Miniflex) under copper radiation (Cu Kα, 30 kV and 15 mA). BET (Brunauer–Emmett–Teller) specific surface area (A_{BET}) and pore size distribution (BJH method) were derived from the nitrogen adsorption–desorption isotherms, which were conducted at 77 K (Quadrasorb SI). The surface functionalized mesoporous silica (SS) with different shapes was named according to aspect ratios. For example, the spherical SS with aspect ratio of 1 was symbolized as SS1.

2.2. Membrane preparation

The PES (RADEL A, Solvay Advanced polymer) was moderately modified with sulfonate functional groups via a sulfonation reaction, following the procedure described in our previous work [24]. The sPES was then used as the polymer matrix for the composite IEMs. The composite membranes were prepared by firstly dissolving 3 g of sPES in 9 g of dimethyformamide (Sigma); then 0–2 wt.% of SS was mixed with the polymer solution at 60 °C for 4 h under stirring. Sonication was applied to the mixture solution before it was cast on glass substrates. The thickness of the casting solution was controlled at 0.40 mm by a "doctor blade" method. The cast film was then dried in a vacuum oven at 60 °C for 10 min to partially remove the solvent and was subsequently precipitated in a 60–70 °C DI water bath. The formed membrane sheets were peeled from the glass substrates and kept in DI water. A series of membranes were named referring to the wt.% of SS added in the polymer matrix. For instance, 0.2SS1 is the abbreviation of the composite membranes of sPES containing 0.2 wt.% of SS with an aspect ratio of 1 (spherical shape). The prepared membranes were treated in hot water for 2 h. All the membranes were equilibrated in a working solution for at least 6 h before use.

2.3. Membrane characterization

2.3.1. Membrane morphology

The morphology and structure of the membranes were observed using scanning electron microscopy (SEM, JEOL 6300). The membrane samples were fractured under liquid nitrogen to obtain a sharp cross-sectional surface, and then the captured water was removed overnight in a freeze dryer to preserve membrane structure.

2.3.2. Ion-exchange capacity (IEC), water uptake, and free volume fraction of IEMs

The IEC of the prepared membranes was measured by a back titration of substituted protons from the sulfonate functional groups of the prepared membranes equilibrated in 1 mol dm^{-3} NaCl solution [25]. The membrane sample 2 × 2 cm in size was equilibrated in DI water for 24 h. The wet weight and dimensions of the membrane were carefully measured before drying in an oven at 50 °C, until there was no change in membrane weight. The dry weight of membrane and dry dimensions were then recorded. The IEC, water uptake, and free-volume fraction of the membranes were calculated using the following equations:

$$IEC = \frac{ab}{W_{dry}} \tag{1}$$

$$Water\ uptake = \frac{W_{wet} - W_{dry}}{W_{dry}} \tag{2}$$

$$Free\ volume\ fraction = \frac{\rho_{wet} - \rho_{dry}}{\rho_w} \tag{3}$$

where a is the concentration of NaOH solution (mol dm^{-3}), b is the volume of NaOH solution used (dm^3), W_{dry} and W_{wet} are the dry and wet weight of the membrane, and ρ_{wet}, ρ_{dry}, and ρ_w are the density of the wet membrane, dry membrane, and water at room temperature, respectively.

2.3.3. Electrochemical properties of IEMs
2.3.3.1. Conductivity of membranes. The resistance of membranes (R_{mem}) in the 0.5 mol dm^{-3} NaCl solution was measured at room temperature by impedance spectroscopy (IS) using a Solarton 225B in a frequency range from 1 to 10^6 Hz with an oscillating

voltage of 100 mV amplitude. Then the conductivity of the membrane (σ, S cm^{-1}) was calculated according to,

$$\sigma = \frac{L}{R_{mem}A} \tag{4}$$

where L is the thickness of membrane (cm) and A is the effective area of the membrane (cm^2).

2.3.3.2. Membrane potential and transport number. Membrane potential was measured in a two-compartment cell, in which a membrane of $1.0\ \text{cm}^2$ effective area separated two NaCl solutions of concentrations 0.01 and 0.05 mol dm^{-3}. The potential difference (E_m) across the membrane was measured at room temperature using a multimeter connected to two Ag/AgCl reference electrodes. The transport number, $\bar{t}_i$, was calculated by:

$$E_m = \frac{RT}{F}(2\bar{t}_i - 1)\ln\left(\frac{C_1}{C_2}\right) \tag{5}$$

where R is the gas constant; F is the Faraday constant; T is the absolute temperature; $\bar{t}_i$ is the transport number of counter ions (ith) in the membranes; C_1 and C_2 are the concentrations of electrolyte solutions in the testing cell, respectively. The ion selectivity of IEM was also presented in terms of membranes permselectivity (P_s), which is defined by;

$$P_s = \frac{\bar{t}_i - t_i}{1 - t_i} \tag{6}$$

where t_i is the transport number of counter ion in the free solution.

2.3.3.3. Current–voltage (i–v) characteristic and chronopotentiometry. The same two-compartment cell connected to a Solartron Multistat 1480 via two Pt electrodes was used to determine the *i–v* curve and chronopotentiogram of the membranes. The experiments were carried out at room temperature using 0.025 mol dm^{-3} NaCl. For the *i–v* curve, the potential difference was applied across the membrane and the corresponding current was measured.

The chronopotentiogram was conducted by constant applied current density of 2.5–3 mA cm^{-2} and the corresponding potential was automatically recorded.

2.3.4. Thermal and mechanical stabilities of membranes

Thermal stability of the membranes was investigated using thermogravimetric analysis (TGA) (Mettler Teledo) under a nitrogen flow of 20 cm^3 min^{-1}, using a heating rate of 10 °C min^{-1} in the range of 25–800 °C.

The mechanical properties of membranes were measured by means of a tensile test in a wet state at room temperature using an Instron 5800, at a speed of 2 mm min^{-1}. Membranes were cut into a rectangular shape with 50 mm × 5 mm dimension. The gauge length of each specimen was set at 14 mm. For acquiring accurate results, at least five specimens from each sample were tested.

2.4. Desalination by electrodialysis (ED)

The desalination performance of prepared membranes was tested in a custom-designed lab-scale ED cell consisting of a 5-compartment chamber made of a Perspex sheet with 4 cm^2 of active area for membranes. An o-ring was used to prevent leakage between each chamber during the process. The scheme of the ED set-up is depicted in Fig. 1.

The ED of NaCl solution was carried out with potentiostatic modes at 7 V. The feed solution (150 cm^3 of 0.2 mol dm^{-3} NaCl) was circulated at 30 cm^3 min^{-1} through the dilute and concentrated compartments. The concentrated compartments were adjacent to the electrode rinse compartments, in which 150 cm^{-3} of 3 wt.% Na$_2$SO$_4$ was circulated at 30 cm^3 min^{-1}. The cation exchange membranes (FKE, FumaTech) were placed next to the electrode to separate the electrode solution from the product solution. The commercial anion exchange membrane (FAA, FumTech) was placed next to the commercial cation exchange membrane toward the anode side, and the investigated membrane was placed next to the one toward the cathode side creating the dilute solution compartment in between. The performances in terms of flux, current efficiency (η), and energy consumption (P) of the prepared membranes, which were defined in Eqs. (7)–(10), will be compared with a commercial membrane.

$$\text{Flux} = \frac{\Delta N}{At} \tag{7}$$

$$\eta = \frac{Fz\Delta N}{n_c \int I dt} \tag{8}$$

$$P = \frac{FzU}{3600\eta M_{\text{NaCl}}} \tag{9}$$

$$\Delta N = C_d^{n-1}V_d^{n-1} - C_d^n V_d^n \tag{10}$$
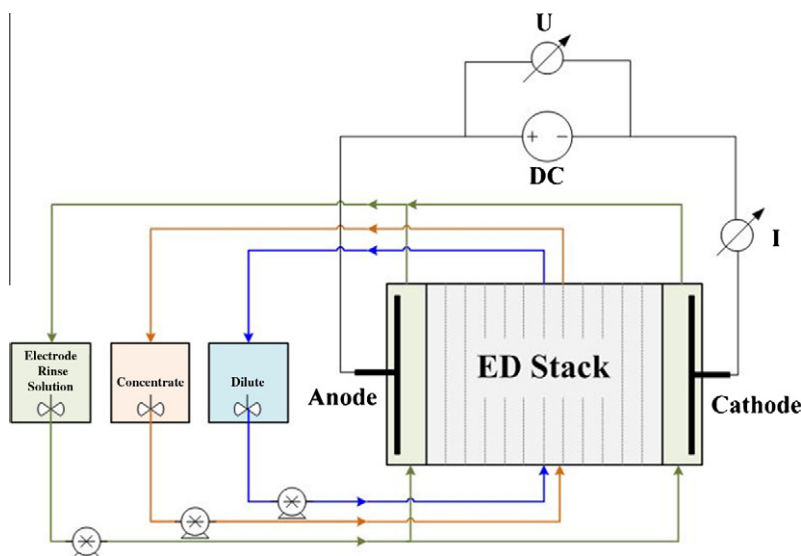
Fig. 1. The schematic experiment set-up of the ED cell.

Table 1
Preparation condition of SS and their properties.

	SS1	SS3	SS10
Chemical composition			
CTAB:PFOA:TEOS:MPTMS:NaOH:H$_2$O	0.13:0:1:0.1:0.31:1200	0.09:0:1:0.1:0.25:920	0.09:0.01:1:0.1:0.25:920
Addition time (s)	5	30	30
Temperature (°C)	80	60	60
Particle size (nm)	⌀100–150	⌀100 × (250–300)	⌀50 × (400–500)
Aspect ratio	1	3	10
A_{BET} (m^2 g^{-1})	942	1002	608
IEC (mequiv g^{-1})	1.80	1.98	1.56

where C_d: Concentration of dilute (mol dm^{-3}); V_d: Volume of dilute (dm^{-3}); n_c: Number of cell pair; I: Current (A); U: Applied voltage (V); M_{NaCl}: Molecular weight of NaCl (58.45 g mol^{-1}); A: Active surface area (cm^2); t: time (s).

3. Results and discussion

3.1. Instinct properties of the inorganic fillers

In this work, mesoporous silica with various shapes and aspect ratios were synthesized for use as inorganic fillers. Table 1 summarizes the preparation conditions and the obtained properties of SS.

More detailed preparation and characterization of these inorganic fillers can be acquired from the literature [18,23]. The obtained particles in each condition were uniform in shape and size as shown by the TEM images (Fig. 2).The aspect ratios of spherical, worm-like, and fiber structures were estimated to be about 1, 3, and 10, respectively, designated as SS1, SS3, and SS10 hereafter. For each sample, the particle size was measured to be about ⌀100–150 nm for SS1, (here ⌀ is the diameter of the spherical particles), ⌀100 × (250–300) nm for SS3 (here ⌀ represents the diameter of fibers, and (250–500) nm represents the length of the fibers), and ⌀50 × (400–500 nm) for SS10, respectively. The small-angle XRD pattern of the spherical and worm-like sulfonated SiO$_2$ (SS1 and SS3) showed well-defined reflections of 2D-hexagonal mesostructure with indexes of (1 0 0), (1 1 0), and (2 0 0), confirming the well-ordered materials. The reflections of worm-like structure (SS3) and mesoporous silica fibers (SS10) showed a small shift to a higher 2θ, and the pore structure was slightly disordered. From the TEM image (Fig. 2c), SS10 appeared to be a well-ordered materials. However, only one broad peak at (1 0 0) was found. This may be due to the short range pore ordering in this sample. Nevertheless, we could conclude from the TEM and XRD results that all the particles were relatively uniform and highly porous. Note that the XRD results were in a good agreement with TEM. Sulfonated groups were attached to the surface of these silica particles in order to provide additional fixed charged functional groups for the sPES matrix and to improve their dispersibility, as mentioned earlier. With the high surface area (600–1000 m^2 g^{-1}) of the porous silica providing available surface for sulfonate groups, a high IEC of the inorganic fillers was resulted. It is worth noting that the IEC of SS10 was lower than those of the SS1 and SS3 due to the less surface area and the discontinued pore channels in the SS10 sample.

3.2. The influence of the inorganic fillers on the membrane microstructures

These surface functionalized SS particles were mixed with polymer solution of sPES to form composite membranes via a two-step
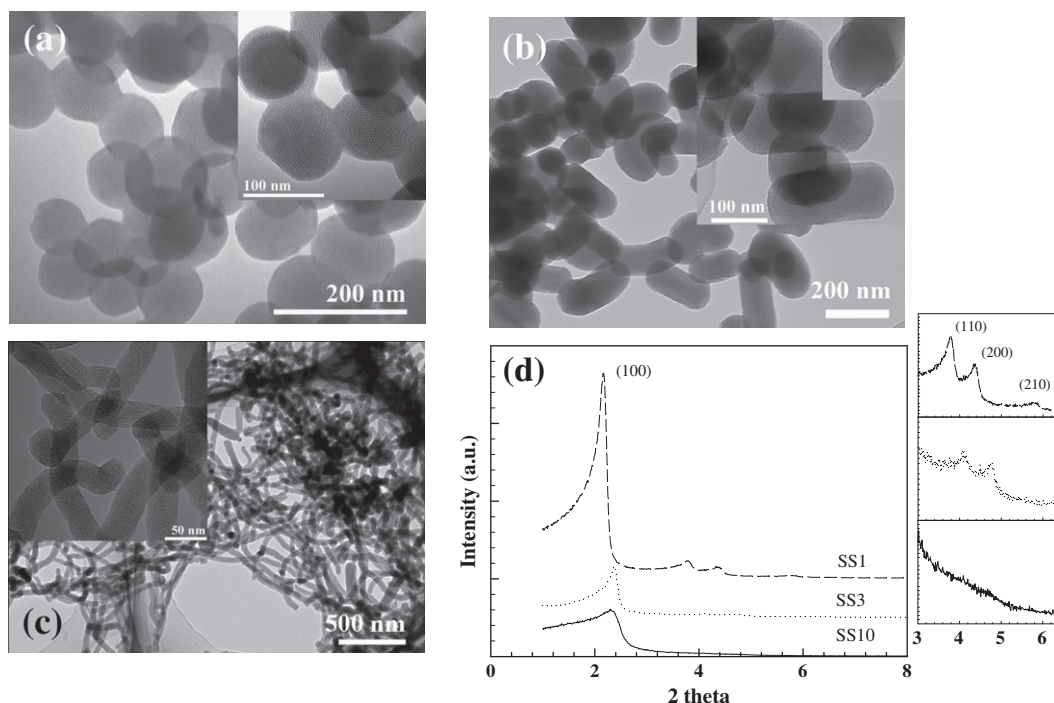
Fig. 2. TEM images of (a) spherical SS with aspect ratio of 1, (b) worm-like SS with aspect ratio of 3, and (c) fiber SS with aspect ratio of 10, and (d) XRD pattern of the synthesized SS. Insets present high-resolution TEM images and XRD patterns of the samples.

phase inversion method by combining both solvent evaporation and precipitation processes. The first evaporation step was introduced to increase the viscosity and concentration of the cast solution, before the step of precipitation in water bath. The phase inversion is one of the most commonly used membrane formation procedures, in which the porosity of the membrane microstructure can be controlled by adjusting the casting solution properties [26–29]. In this work, when the fillers with different aspect ratios were added into the matrix solution, the incompatibility between the two components created polymer-depleted phase around the inorganic phase, which facilitates the porosity formation during the phase inversion process [21]. This was clearly evident from the SEM images of the resultant composite membranes (Fig. 3). The porosity of the composites was increased compared with that of the parent polymer membrane (Fig. 3m).

Due to the apparently interfacial interaction between polymer matrix and inorganic fillers with various aspect ratios, composite membranes with different porosities were obtained (Fig. 3). At lower SS content (0.2 wt.%, 0.5 wt.%), the SS10 sample showed less porosity in comparison with other composites SS1 and SS3, possibly due to the better polymer–filler interaction in SS10 sample. It was interesting to see that SS3 sample had quite significant porosity

in comparison with that of SS1 (Fig. 3e–h), which might be attributed to the higher surface functional groups of the SS3 that could have significant influence on the interfacial interaction between polymer and the fillers.

When more SS was added in the polymer matrix, the particles tended to form clusters and thus larger pores were created due to the worse polymer–filler clusters/aggregates interaction. As shown in Fig. 3 with more than 1 wt.% SS loading, the large cavities with pore interconnection were obtained. Note that in case of the fillers with higher aspect ratio, they tended to form bigger clusters and create larger pores subsequently due to their poorer dispersing ability. Thus the formation of porosity of the composite membranes can be quite complicated, possibly due to the following several effects: (1) the porosity of the polymer–filler interfacial gap, (2) the inherit properties and porosity of the fillers, and (3) the extra functional groups carried by the fillers. These synergetic effects eventually led to the composites with varied porosities, depending upon the addition amount and aspect ratio of the fillers.

The formation of these large pores would finally affect the mechanical stability of the membranes. The mechanical properties of these membranes were investigated under wet conditions, and the results are illustrated in Fig. 4a–c. In most cases, the Young's
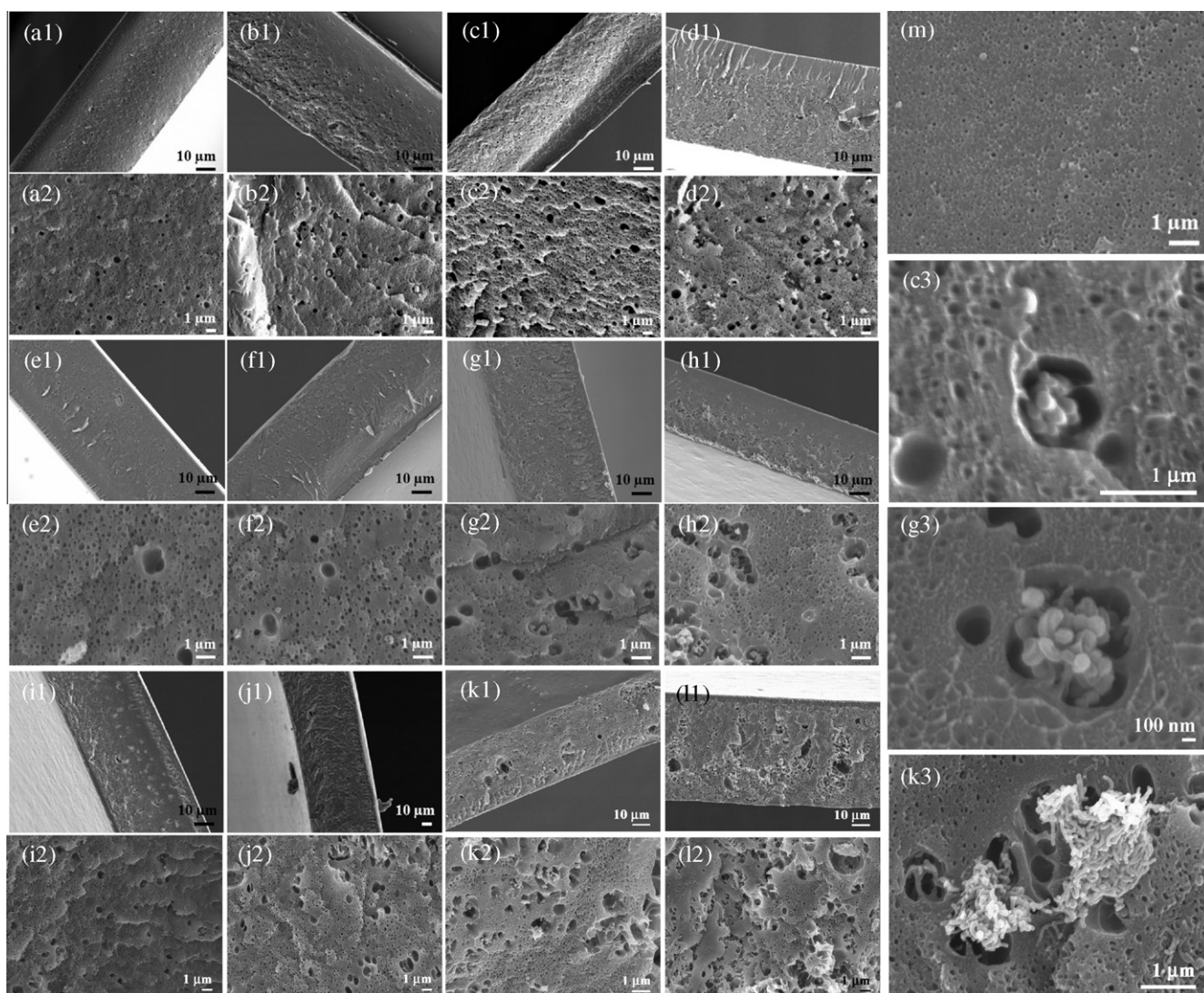
Fig. 3. SEM images of sPES-based composite membranes containing (a–d) 0.2, 0.5, 1, and 2 wt.% SS1, (e–h) 0.2, 0.5, 1, and 2 wt.% SS3, (i–l) 0.2, 0.5, 1, and 2 wt.% SS10, and (m) pristine sPES membrane.

modulus of the composites was decreased with increasing filler amount, while the average values were still higher than that of pristine sPES membranes. This could be attributable to the increased elongation and elastic properties of the composites. When a lower amount of SS was added, the fillers with a higher aspect ratio developed better interface interaction, and thus better distributed the force between the filler and the matrix, resulting in higher strength [20]. However, at higher filler content, membranes became stiffer and with more than 1 wt.% SS loading, the loss of membrane structure was more pronounced due to the particle aggregation and the formation of larger pores. Thermal stability of these dried composites was also studied by TGA (Fig. 4d).

The weight change at temperatures lower than 100 °C can be assigned to the loss of absorbed water. The membranes started to decompose slowly at around 280 °C due to the loss of sulfonate groups. A sharp weight loss occurred at around 500 °C when the polymer main chains were decomposed. As the inorganic additives were incorporated into the polymer matrix, the composites showed improved thermal stability. Interestingly, it is apparent that thermal stability slightly increased with increasing the aspect ratio of the fillers, which may be attributed to greater contact and interaction between the flillers and the polymer matrix.

3.3. Membrane properties

The properties of the as-synthesized membranes were investigated as summarized in Table 2. Compared to the pristine membrane, the composites showed an overall improvement in properties. Especially, the conductivity of the membranes was improved up to 10–20 folds. This is mainly due to the increased porosity and water channels in the membrane structures by adding the inorganic fillers, which facilitate the migration of ionic species.

Further to the discussion in earlier section on the influence of the aspect ratio on membrane structures, the increased porosity of the composite can also be interpreted by the term "free-volume fraction," which is the fraction of the absorbed water in the membrane

Table 2
Properties of composite membranes compared with commercial membrane, FKE.

Name	Water uptake (%)	IEC (mequiv g^{-1})	σ (mS cm^{-1})	Transport number	Free-volume fraction	P_s (%)
0S	38.67	0.75	0.336	0.90	0.43	83.61
0.2SS1	92.00	0.83	5.554	0.95	0.74	91.81
0.5SS1	85.00	0.78	1.460	0.95	0.70	91.81
1.0SS1	79.00	0.73	1.330	0.96	0.69	93.45
2.0SS1	55.00	0.69	0.960	0.91	0.67	85.25
0.2SS3	100.5	0.85	6.695	0.92	0.73	86.89
0.5SS3	97.47	0.67	3.300	0.94	0.67	90.17
1.0SS3	72.91	0.66	3.112	0.81	0.62	68.87
2.0SS3	71.30	0.65	2.878	0.76	0.62	60.68
0.2SS10	56.52	0.78	1.910	0.99	0.53	95.08
0.5SS10	74.73	0.69	3.710	0.96	0.54	93.45
1.0SS10	89.73	0.69	3.870	0.86	0.59	77.06
2.0SS10	96.08	0.66	3.770	0.68	0.66	47.57
FKE	48.10	1.20	3.834	0.95	N/A	91.81

pore to the total membrane volume. For instance, the free-volume fractions of the composites were apparently larger than that of parent sPES membrane. At low SS loading amount, the water uptake in SS10 composite was lower than that of other membranes due to better polymer–filler interaction. The conductivity of the membrane was improved, following the same trend as water uptake because the water channels assist the migration of ionic species.

Ion-exchange capacity, which reflects the amount of charged functional groups, is normally related closely to the selectivity and conductivity in the dense IEMs, increased with increasing SS amount and peaked at 0.2 wt.% SS loading. While at low additive content, the particles were dispersed and distributed uniformly in the polymer matrix (as mentioned in previous section), at higher filler concentration, the particles started to form aggregated clusters. Consequently, their surface functional groups were partially inaccessible, and these clusters started to interrupt chain arrangement of the polymer matrix, resulting in lower IEC. Transport number,
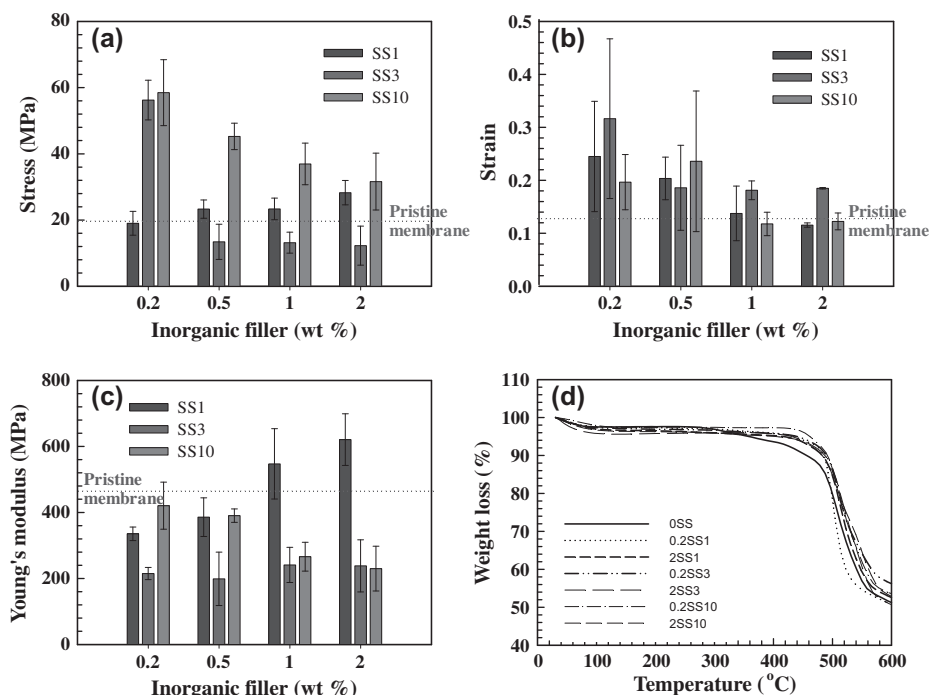
Fig. 4. Mechanical properties of the prepared membranes; (a) tensile stress, (b) tensile strain and (c) Young's modulus, and (d) TGA of some selected composites as a representative of their series. Dotted lines (a–c) indicate the average mechanical property of pristine membrane.

the value representing the fraction of current carried by counter charges through membranes, which can also be expressed in the term of permselectivity (P_s), was also improved by incorporating SS. This is because SS carries additional charged functional groups, and thus helps the Donnan exclusion to work more effectively. However, the porosity and structure of the membranes and their selectivity have to be carefully compromised. At high loading, larger pores were formed in the membranes. These large cavities were filled by equilibrium electrolyte solution that allows both ionic species and solvent to transport across the membranes, resulting in less selective behavior [30]. In the case of spherical particles (SS1), the transport number and permselectivity increased with increasing SS loading and peaked at around 1 wt.% loading. However, for SS3 and SS10, the peak was observed at lower percent loading at around 0.2–0.5%. This is mainly due to the larger pore sizes and lower charge density that reduce the Donnan exclusion effect.

In summary, the properties of the newly developed composite membranes were improved, and a number of membranes exhibited comparable parameters as that of the benchmark membrane, FKE. This clearly indicates the amount and shape of inorganic fillers play important roles in tuning the key parameters of ion-exchange membranes.

3.4. Chronopotentiogram and surface heterogeneity of the composite membranes

To develop new membrane for the electrically driven processes, it is important to understand the electrochemical properties of membranes. In this work, we used chronopotentiometry to determine the degree of surface heterogeneity, which is believed to greatly influence the electrochemical properties and polarization phenomena of membranes [31]. Representative chronopotentiograms obtained at low inorganic loading are shown in Fig. 5.

A three-stage potential response to application of constant current density through the system was typically observed. The first stage shows a nearly constant potential that is due to a decrease in the concentration of the depleted solution and increased concentration in the adjacent side of the membrane. When the ionic concentration of the depleted solution drops to near zero, the potential suddenly increases before reaching the final steady state. The point at which the sharp increase in potential occurs is called transition time (τ), which can be expressed in the well-known Sand equation, based on the assumption of homogeneous ionic solution:

$$\tau = \frac{(C_0 z_i F)^2 \pi D}{4 i^2 (\bar{t}_i - t_i)^2} \tag{11}$$

where i is the current density, C_0 is the concentration of electrolyte, z_i is the valence of the ith ion, and D is the diffusion coefficient. The characteristic values of the transition time are summarized in Table 3. In practical terms, IEM is considered heterogeneous on the microscale, consisting of a conducting and non-conducting phases. The transition times estimated from Eq. (11) were higher than those obtained from the chrononpotentiograms. This may be due to the local current density of the heterogeneous membranes near the reduced conducting region being higher than the overall current density of the entire surface, resulting in faster depletion of the ionic species [7,31,32]. The fraction of the conducting region, ε, can be estimated by replacing the overall current density (i) with the local current density in the conducting region (i/ε) in Eq. (11). Using the Sand equation, ε can be expressed as follows;

$$\varepsilon = \frac{2 i \tau^{1/2} (\bar{t}_i - t_i)}{C_0 z_i F (\pi D)^{1/2}} \tag{12}$$
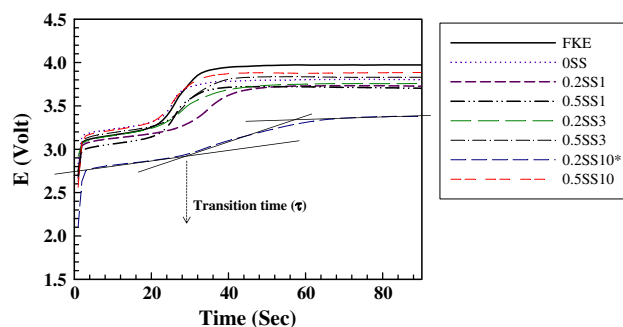
Fig. 5. Chronopotentiograms of composite membranes containing low SS wt.% compared with pristine and commercial membranes conducted at room temperature in 0.025 mol dm^{-3} NaCl under constant applied current density of 3.0 mA cm^{-2}. Note that the 0.2 SS10 membrane was tested under lower current density of 2.5 mA cm^{-2} due to its lower limiting current density.

The results from the chronopotentiograms indicate that small amount of charged inorganic fillers increased the conducting region of the membrane surfaces. However, when the SS loading was more than 1 wt.%, the agglomerates created separated phases due to significant charge interaction and surface heterogeneity on the membranes. Note that the deviation of the transition time in chronopotentiogram and from that predicted by the Sand equation was smaller, when surfaces of the membranes were more homogeneous and conductive.

3.5. Current–potential curve and concentration polarization of membranes

The current–potential characteristics are well-known indication of chemical polarization near the membrane interface. In the electrodriving process, for example, in desalination by electrodialysis, when potential is applied across the system, ionic species migrate toward the opposite pole, passing through ion-selective membranes that allow the counter ion to pass through and reject the co-ions. Due to the difference in transport of ions through membranes and electrolyte solutions, the solution concentration near the membrane interface decreases on one side and increases on the other side of the membrane. Once the concentration of the depleting solution reaches zero, the concentration polarization has a dramatic effect on the transport phenomena of membranes, normally leading to a loss of current efficiency [6]. In a severe case,

Table 3
Characteristic values from chronopotentiogram and i–v curve.

Name	$\bar{t}_i$	τ^a	τ^b	ε	i_{lim} (mA cm^{-2})	i^* (mA cm^{-2})	ΔE (V)
0SS	0.90	32.18	22.00	0.864	2.19	2.54	1.60
0.2SS1	0.95	26.63	30.00	0.997	2.21	2.21	0.94
0.5SS1	0.95	26.63	22.50	0.997	2.04	2.04	0.67
1.0SS1	0.96	25.70	25.00	0.946	2.21	2.33	0.53
2.0SS1	0.91	30.94	22.00	0.862	2.08	2.41	0.70
0.2SS3	0.92	29.77	27.00	0.952	2.40	2.52	1.20
0.5SS3	0.94	28.13	28.00	0.998	2.12	2.12	1.07
1.0SS3	0.81	47.69	42.00	0.938	2.25	2.40	0.67
2.0SS3	0.76	61.70	27.00	0.662	2.70	4.08	0.94
0.2SS10	0.99	23.16^c	33.00^c	0.956	2.00	2.09	1.32
0.5SS10	0.96	37.01	25.00	0.979	2.05	2.09	0.68
1.0SS10	0.86	37.97	28.00	0.855	2.13	2.49	0.93
2.0SS10	0.68	101.4	37.00	0.604	2.50	4.14	0.94
FKE	0.95	26.63	26.00	0.988	2.06	2.08	0.80

^{a} Estimated from Eq. (11).
^{b} Deprived form chronopotentiogram.
^{c} Measured at 2.5 mA cm^{-2}.

this may lead to pH change due to water dissociation, which will promote scale formation and damage to the membranes. Thus, further increasing the driving force will not further improve the efficiency of the system. Therefore, it is important to know the limiting point of the operating conditions. The current density at which drastic concentration polarization occurs, known as the limiting current density (LCD, i_{lim}), can be estimated experimentally from the i–v curve and theoretically via Eq. (13) based on classical polarization theory:

$$i_{lim} = \frac{|z|CFD}{\delta(\overline{t_i} - t_i)} \tag{13}$$

Fig. 6 shows the representative i–v curves from composites at low percent loading of SS in each series compared to a commercial membrane (FKE). Typical i–v curves with three stages of potential change were obtained; (1) the Ohmic region at the beginning when the potential varies with current according to the Ohms' law; (2) plateau region caused by concentration polarization, and (3) the overlimiting potential region, where the transport phenomena of the IEM depends mainly on electroconvection phenomena. In general, shape and plateau length of the IEM depends on many factors and is strongly influenced by the structure of the membranes and their surface heterogeneity [33]. Membranes with favorable surface homogeneity will provide a well-defined plateau region. The LCD and characteristic values of all membranes are summarized in Table 3.

Compared to the pristine membrane, the composite membranes possessed higher LCD. It is worth noting that theoretically the LCD is proportional to the reciprocal of transport number as defined by Eq. (13) under the same testing conditions. However, the results revealed the opposite trend. This can be explained by the locally higher current density (i^*) of the reduced conducting surface in the microheterogeneous model. The limiting current density (i_{lim}) obtained experimentally and the current density near conducting region with applied correction factor (fraction of conducting region of the membrane surface ($i^* = i_{lim}/\varepsilon$)) were also listed in Table 3. As can be seen from the results, after taking the fraction of conducting region into account, the membranes with lower transport number exhibited higher i^* as expected theoretically following the classical polarization theory. It was clear that the presence of a small amount of SS enhanced the fraction of conducting surface and electrochemical properties and also increased the LCD, offering advantages for ED application.

3.6. Desalination of NaCl by ED

The preliminary ED tests of some selected membranes were displayed in this section. The performance of a membrane in ED
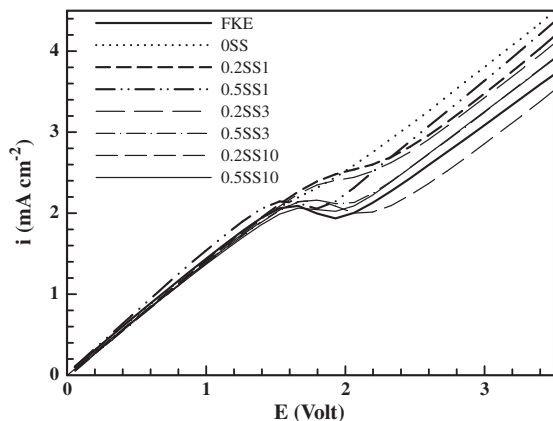
Fig. 6. i–v Curve of composite membranes at low wt.% fillers compared with a commercial membrane.

Table 4
Desalination performances by ED with composite membranes and FKE membrane.

Membrane	Flux (Mole m^{-2} h^{-1})	η	P (kW h kg^{-1} salt)
FKE	7.7	0.84	3.80
0SS	4.3	0.53	5.89
0.2SS1	6.7	0.84	3.83
0.2SS3	7.1	0.95	3.18
0.2SS10	5.3	0.87	3.69
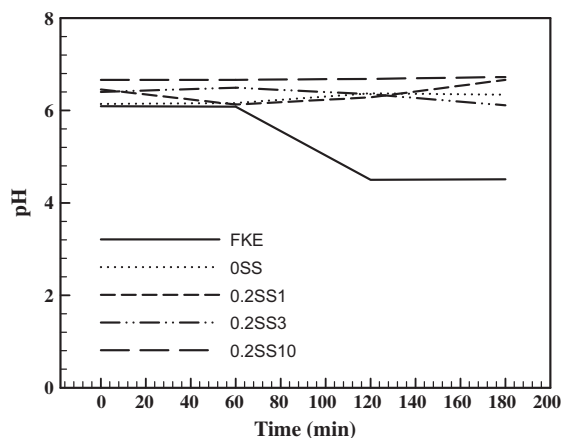
Fig. 7. pH values of depleting solutions from ED test.

application depends not only on the properties of the tested membranes but also the operating conditions and the cell design. The composites with low additive loading (0.2 wt.%) from each series were selected to desalt the monoelectrolyte solution, NaCl, using our home-designed lab-scale ED cell. The performances of the membranes in terms of flux, energy consumption, and current efficiency are summarized in Table 4. Note that each experiment was carried out for 3 h, and the values shown here were estimated at the final stage of the experiment.

Note that the term "flux" in this work refers to the amount of salts removed per unit active area of membrane in a given time. It was encouraging to see that with significant improvement in conductivity and transport number, the composite membranes showed much better performance in ED compared with the pristine sPES membrane. In the case of the SS3 composite membranes, the overall performance was even slightly better than the commercial FKE one. Moreover, as mentioned earlier, our composite membranes have improved LCD, allowing these materials to operate at higher potential difference without reducing current efficiency. The more the driving force applied, the better the performance expected. With the same operating potential, the pH of the diluted solution treated by the commercial membrane became acidic after a short time of operation (see Fig. 7), indicating that this membrane may have already undergone water dissociation, while the pH of treated solution from our prepared membranes remained nearly constant.

4. Conclusions

A new type of inorganic–organic nanocomposite IEMs was successfully prepared. The presence of inorganic fillers had a significant impact on the structure of the membrane, which in turn affected the overall membrane properties. It was evidenced that inorganic fillers, carrying extra functional groups for the organic polymer matrix, enhanced overall physicochemical and electrochemical properties including water uptake, IEC, conductivity,

transport properties, and conducting fractions of the membrane surface, while maintaining good mechanical and thermal stability of the parent matrix. The shape of inorganic fillers strongly influenced the membrane structure and properties of the composite membranes. The optimized composite exhibited comparable performances in ED of the benchmark commercial membrane.

Acknowledgments

References

[1] R. Scherer, A.M. Bernardes, M.M.C. Forte, J.Z. Ferreira, C.A. Ferreira, Mater. Chem. Phys. 71 (2001) 131–136.
[2] C. Iojoiu, M. Marechal, F. Chabert, J.-Y. Sanchez, Fuel Cells 5 (2005) 344–354.
[3] N.N. Krishnan, H.-J. Kim, M. Prasanna, E. Cho, E.-M. Shin, S.-Y. Lee, I.-H. Oh, S.-A. Hong, T.-H. Lim, J. Power Sources 158 (2006) 1246–1250.
[4] S. Feng, Y. Shang, X. Xie, Y. Wang, J. Xu, J. Membr. Sci. 335 (2009) 13–20.
[5] G.S. Gohil, R.K. Nagarale, V.V. Binsu, V.K. Shahi, J. Colloid Interface Sci. 298 (2006) 845–853.
[6] J. Balster, O. Krupenko, I. Punt, D.F. Stamatialis, M. Wessling, J. Membr. Sci. 263 (2005) 137–145.
[7] M.-S. Kang, Y.-J. Choi, I.-J. Choi, T.-H. Yoon, S.-H. Moon, J. Membr. Sci. 216 (2003) 39–53.
[8] A. Elatar, A. Elmidaoui, N. Pismenskaia, C. Gavach, G. Pourcelly, J. Membr. Sci. 143 (1998) 249–261.
[9] H.K. Hansen, L.M. Ottosen, A. Villumsen, Sep. Sci. Technol. 34 (2008) 2223–2233.
[10] Y.S. Dzyazko, V.N. Belyakov, Desalination 162 (2004) 179–189.
[11] Y.S. Kim, M.A. Hickner, L. Dong, B.S. Pivovar, J.E. McGrath, J. Membr. Sci. 243 (2004) 317–326.
[12] M. Sankir, V.A. Bhanu, W.L. Harrison, H. Ghassemi, K.B. Wiles, T.E. Glass, A.E. Brink, M.H. Brink, J.E. McGrath, J. Appl. Polym. Sci. 100 (2006) 4595–4602.
[13] C. Xu, T. Xu, W. Yang, J. Membr. Sci. 224 (2003) 117–125.
[14] R.K. Nagarale, G.S. Gohil, V.K. Shahi, R. Rangarajan, Macromolecules 37 (2004) 10023–10030.
[15] V. Ganesan, A. Walcarius, Langmuir 20 (2004) 3632–3640.
[16] D. Gomes, R. Marschall, S.P. Nunes, M. Wark, J. Membr. Sci. 322 (2008) 406–415.
[17] R. Marschall, I. Bannat, J. Caro, M. Wark, Microporous Mesoporous Mater. 99 (2007) 190–196.
[18] R. Marschall, I. Bannat, A. Feldhoff, L. Wang, G.Q.M. Lu, M. Wark, Small 5 (2009) 854–859.
[19] M. Wilhelm, M. Jeske, R. Marschall, W.L. Cavalcanti, P. Tolle, C. Kohler, D. Koch, T. Frauenheim, G. Grathwohl, J. Caro, M. Wark, J. Membr. Sci. 316 (2008) 164–175.
[20] L. Chazeau, C. Gauthier, G. Vigier, J.Y. Cavaille, Relationships between microstructural aspects and mechanical properties of polymer-based nanocomposites, in: H.S. Nalwa (Ed.), Handbook of Organic–Inorganic Hybrid Materials and Nanocomposites, American Scientific Publishers, 2003.
[21] M.A. Aroon, A.F. Ismail, T. Matsuura, M.M. Montazer-Rahmati, Sep. Purif. Technol. 75 (2010) 229–242.
[22] S. Basu, A.L. Khan, A. Cano-Odena, C. Liu, I.F.J. Vankelecom, Chem. Soc. Rev. 39 (2010) 750–768.
[23] F. Rambaud, K. Valle, S. Thibaud, B. Julian-Lopes, C. Sanchez, Adv. Funct. Mater. 19 (2009) 2896–2905.
[24] C. Klaysom, R. Marschall, B.P. Ladewig, G.Q.M. Lu, L. Wang, J. Mater. Chem. 20 (2010) 4669–4674.
[25] C. Klaysom, B.P. Ladewig, G.Q.M. Lu, L. Wang, J. Membr. Sci. 368 (2011) 48–53.
[26] C. Barth, M.C. Goncalves, A.T.N. Pires, J. Roeder, B.A. Wolf, J. Membr. Sci. 169 (2000) 287–299.
[27] J. Barzin, B. Sadatnia, Polymer 48 (2007) 1620–1631.
[28] A. Conesa, T. Gumi, C. Palet, J. Membr. Sci. 287 (2007) 29–40.
[29] P. Van de Witte, P.J. Dijkstra, J.W.A. Van de Berg, J. Feijen, J. Membr. Sci. 117 (1996) 1–31.
[30] N.P. Gnusin, N.P. Berezina, N.A. Kononenko, O.A. Dyomina, J. Membr. Sci. 243 (2004) 301–310.
[31] J.-H. Choi, S.-H. Kim, S.-H. Moon, J. Colloid Interface Sci. 241 (2001) 120–126.
[32] J.-H. Choi, S.-H. Moon, J. Membr. Sci. 191 (2001) 225–236.
[33] V.M. Aguilella, S. Mafe, J.A. Manzanares, J. Pellicer, J. Membr. Sci. 61 (1991) 177–190.